Synthesis and characterisation of fluorenone–thiophene-based donor–acceptor oligomers: role of moiety sequence upon packing and electronic properties†

William Porzio,*[a] Silvia Destri,*[a] Mariacecilia Pasini,[a] Umberto Giovanella,[a] Massimo Ragazzi,[a] Guido Scavia,[a] Dariusz Kotowski,[a] Gianni Zotti[b] and Barbara Vercelli[b]

Received (in Montpellier, France) 20th January 2010, Accepted 14th April 2010
DOI: 10.1039/c0nj00045k

A series of oligomers constituting alternating thiophene and fluorenone residues, designed to evaluate the effect upon both electronic properties and packing of the moiety sequence in the light of donor–acceptor concept, were synthesised and studied by cyclic voltammetry, optical spectroscopy, and XRD investigations into crystals, films, and powders. Moreover, *ab initio* calculations, based on Density Functional Theory, were carried out on selected molecules. A clear indication of close-packing induction by fluorenone in the oligomers, together with the factors determining the electrical and optical properties, are derived and presented. In the light of the performance of selected compounds in prototypes of p-type FET devices and bulk heterojunction solar cells, some general indications of chemical structure requirements for applications such as photovoltaic cells are described.

1. Introduction

The role of oligomers and polymers based on fluorenone (**F**) and thiophene (**T**)/aromatic residues in optoelectronics has recently received attention in the literature.[1–9] In summary, **F**-based polymers[2] and copolymers[3,4] display emission properties and have been considered in light-emitting diodes (LEDs), with the possibility of emitting white light if blended with other molecules.[5] More recently, the **F** moiety has been used as a minor component in blue-emitting copolymers[6,7] and, when added in strictly controlled amounts, as a stabilizer against oxidation.[8] In addition, non-linear optical properties of truxenone derivatives were recently reported,[10] as well as V-shaped liquid-crystals,[11] and a series of **F**-containing oligomers was tested with fullerene as a solar-cell-active material.[12] Finally oligomers or polymers comprising the same residues have been reported as quite good candidates for p- and n-type organic field-effect transistor (OFET) materials, displaying significant electron and hole transport.[13–16]

Indeed, the **F** moiety has been often seen as an irregularity of polyfluorene chains – due to oxidation – resulting in a modified spectral response: namely it decreases its luminescence efficiency,[17,18] yielding a green peak in the emission spectrum. In fact, the **F** moiety, in contrast to fluorene, is stable to oxidation and is capable of close-packing, resulting from H-bond interactions between adjacent molecules.[19]

Such a scenario clearly indicates that the optoelectronic properties would change depending on the sequence of **F** and **T** (or other) residues, raising the prospect of tailoring these materials towards different applications.

As predicted by detailed *ab initio* calculations[20] and verified in many oligomeric arrangements,[13,19,21–25]crystal structures with an extended π-conjugated systems favor charge transport, particularly when strong H-interactions are established, *via* the enhancement of crystal packing factor (PF), being a reliable measure of closeness of packing arrangement. It is commonly established that, together with the chemical nature of the molecule, PF addresses both the molecular orientation with respect to the electrodes, induced at the substrate interface, and also crystal dimensions – and hence electric transport performances.[13,19,21–26]

This paper presents a series of **T**–**F** oligomers, illustrated in Scheme 1, some of which were previously used for the fabrication of p-type OFET devices.[13,14] The considered molecules consist of the alternation of $\mathbf{T}_n$ (n = 1–6) (donor, D) and **F** (acceptor, A) moieties (according to the concept introduced by Havinga[27] and subsequently developed by Curtis[28]) to tune the electronic energy levels, and thus determining stability, spectral window, and the materials used for the electrodes, the work function for which has to match the energy levels.[20,21,24,29,30] In this respect, it is relevant to evaluate these electronic levels, *i.e.* by comparing *ab initio* calculations with experimental determinations such as electrochemical measurements.

For these reasons, both the electrochemical properties (related to Density Functional Theory (DFT) calculations on most D and A examples) and the packing in the molecule series were studied in order to tailor each molecule to a specific

[a] *Istituto CNR per lo Studio delle Macromolecole, via E. Bassini 15, 20133, Milano, Italy.*
E-mail: w.porzio@ismac.cnr.it, s.destri@ismac.cnr.it
[b] *Istituto CNR per l' Energetica e le Interfasi, c.o Stati Uniti 4, 35127 Padova, Italy*

† Electronic supplementary information (ESI) available: MS and NMR spectra; electrochemistry data; FTIR characterisations; field-effect transistor performances; preparation of bulk heterojunction solar cells; crystal structure data. CCDC reference number 736650. For ESI and crystallographic data in CIF or other electronic format see DOI: 10.1039/c0nj00045k

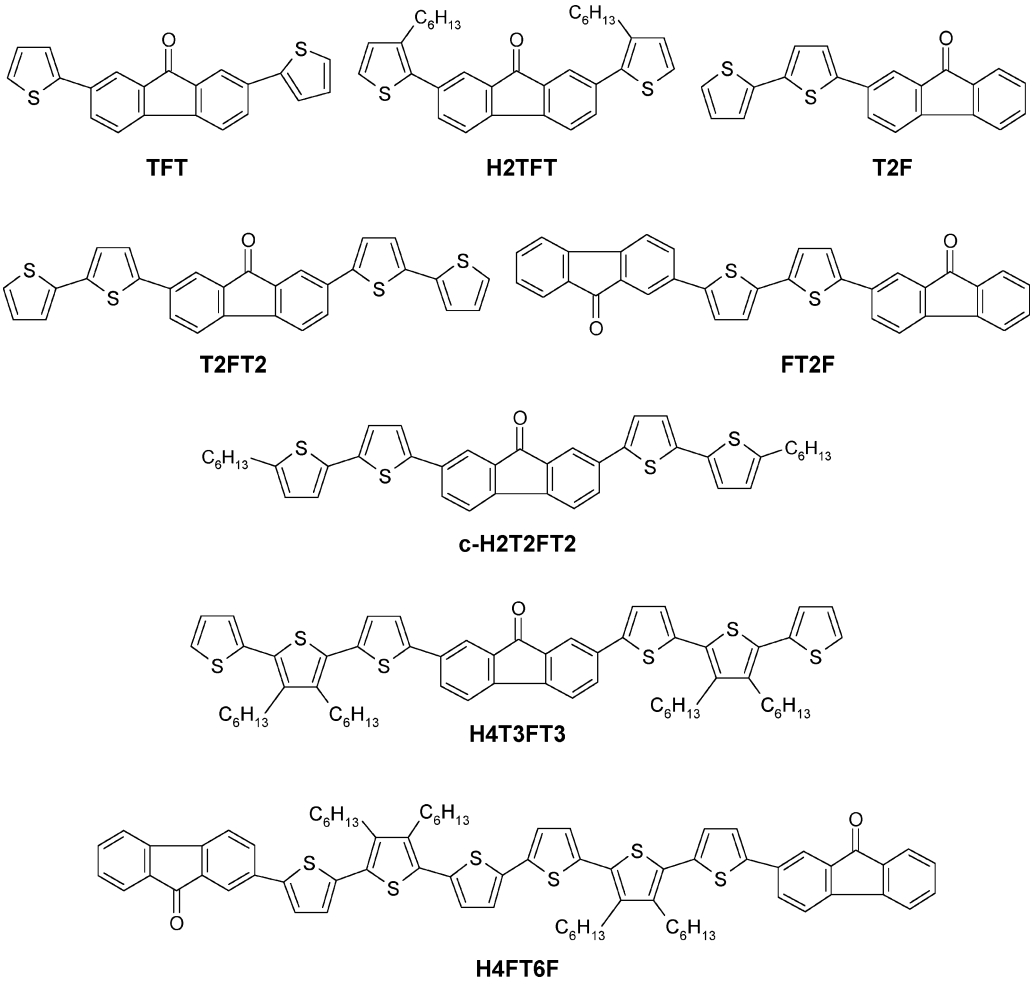

Scheme 1 The molecules prepared and studied.

potential use, *i.e.* OFETs and solar cells. With this aim, we have characterized by cyclic voltammetry, FTIR, light absorption and emission spectroscopy, the oligomers and the corresponding polymers of the molecules that irreversibly oxidize.

X-ray diffraction (XRD) analysis on crystals, powders, and thin films and atomic force microscopy (AFM) characterization have been performed to shed light on the solid-state arrangement, which is related to charge transport capability. Finally, the electrical properties of p-type OFET devices, based on the oligomer examples reported here, and the optoelectronic property in a bulk heterojunction (BHJ) solar cell based on an oligomer and a fullerene derivative, are considered in terms of the above-mentioned factors.

2. Results and discussion

2.1 Chemistry

Different joinings of **T** and **F** units in the oligomers, as well as their number, strongly affect the chemical, electrochemical, and optical properties of the materials. Catalyzed couplings through organometallic compounds and electrosynthesis offer the possibility to prepare the molecules reported in Scheme 1. 2,7-(2-Thienyl)-9-fluorenone (**TFT**),[13] 2,7-di(5-*n*-hexyl-2,2′-bithienyl)fluoren-9-one (**c-H2T2FT2**)[14] and 5,5′-(2,7-fluoren-9-onyl)-2,2′-bithiophene (**FT2F**)[13] were prepared according to the literature. 2,7-Di(2,2′-bithienyl)-9-fluorenone (**T2FT2**) and 2,7-di(3-*n*-hexylthien-2-yl)fluoren-9-one (**H2TFT**) were obtained by Suzuki coupling of 2,7-dibromofluoren-9-one with 5-(4,4,5,5-tetramethyl-1,3,2-dioxaborolan)-2,2′-bithiophene and 2-(4,4,5,5-tetramethyl-1,3,2-dioxaborolan)-3-*n*-hexylthiophene respectively. Monobromofluorenone reacted according to the standard coupling conditions for the preparation of (2,2′-bithien-5-yl)-9-fluorenone (**T2F**).

As reported in Scheme 2, to synthesize 2,7-di(3′,4′-di-*n*-hexyl-2,2′,5′,2″-terthienyl)fluoren-9-one (**H4T3FT3**) the thiophene trimer 3′,4′-dihexyl-2,2′;5′,2″-terthiophene was prepared in good yield (70%) by Stille coupling of 2,5-dibromo-3,4-dihexylthiophene and 2-tributylstannylthiophene.[31] The reaction (*via* lithiation) of the terthiophene with 2-isopropoxy-(4,4,5,5-tetramethyl)-1,3,2-dioxoborolane gave an intermediate that reacted immediately with 2,7-dibromofluoren-9-one using the Suzuki reaction, without any purification.

The reaction with 2-bromofluorenone gave the monomer **H2T3F**, which was dimerized by exhaustive electrolysis to **H4FT6F** in quantitative yield.[32]

 This journal is © The Royal Society of Chemistry and the Centre National de la Recherche Scientifique 2010

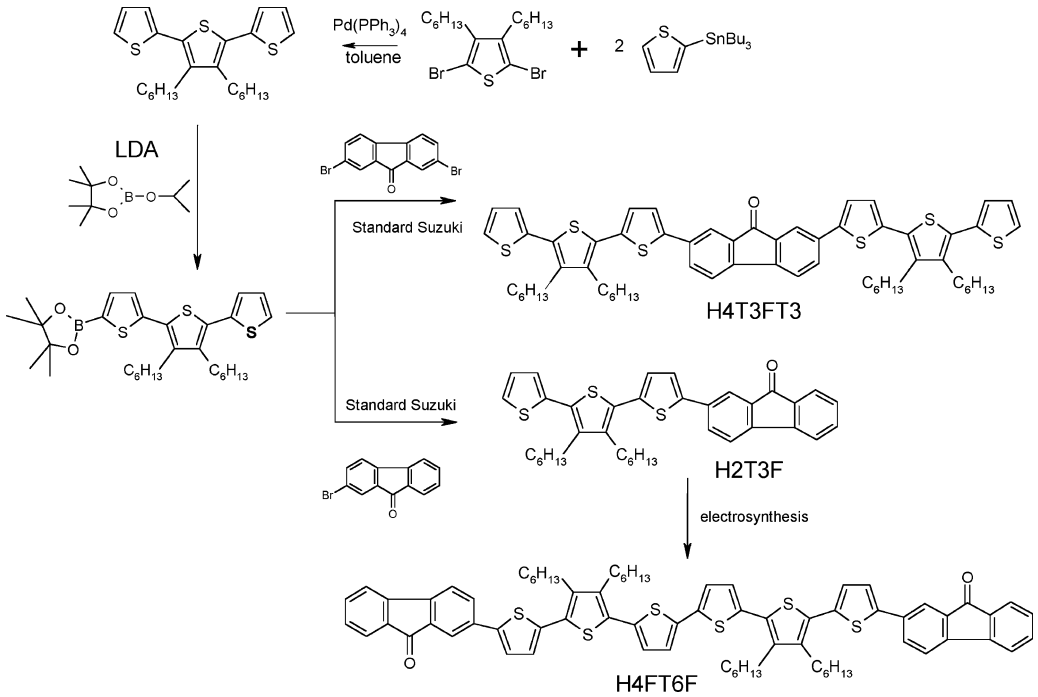

Scheme 2 Reaction pathway for the synthesis of the studied molecules.

2.2 Electrochemistry

The compounds were generally investigated in millimolar concentrations in acetonitrile + 0.1 M Bu_4NClO_4. Methylene chloride and chlorobenzene were used for **H4T3FT3** and **T2FT2** respectively for solubility reasons. Electrodeposited films were in all cases investigated in acetonitrile + 0.1 M Bu_4NClO_4. Electrochemical (CV peak at 0.1 Vs^{-1} or redox potentials) parameters for the investigated compounds and coupling products are summarized in Table 1. All the potentials quoted in this paper are referred to the Ag/Ag^+ 0.1 M electrode.

The electrochemical behaviour can be to some extent anticipated by the known electrochemistry of the co-monomer units. The oxidation potentials of **T**, **T2**, and **T3** are 1.73, 0.97 and 0.71 V[33] respectively and that of **F** is 1.70 V.[34] 3-Methylthiophene, a representative 3-alkylsubstituted thiophene, shows an irreversible oxidation cyclic voltammogram (CV) peak at E_p = 1.46 V,[35] so alkyl substitution makes the **T** ring electron-rich compared with **F**. From these values, it is clear that for 3-alkylthiophenes, **T2**, **T3**, and the fluorenone derivatives of Scheme 1, oxidation is localized at the thiophene moiety.

The molecules can be divided into three classes depending on the presence of capping groups.

FT2F and **c-H2T2FT2** are **T-F** compounds where two fluorenone residues are the outer moieties and both the bithien-2-yl residues are capped in the 5′-position. The CV of **FT2F**, *i.e.* the **F-T2-F** subunit, as a cast film shows reversible oxidation at the same E^0 value (as average of forward and backward peak potentials) as for **poly(TFT)** (see below), as expected. The CV of **c-H2T2FT2**, *i.e.* the end-capped **T2FT2** subunit, as a film shows a partially reversible oxidation process

Table 1 Molecule oxidation and reduction peak potentials (E_m^p) in solution, polymer film oxidation and reduction peak potentials (E^0) together with their ΔE as difference between oxidation and reduction peak potentials, and E_g^{OPT} values

Monomer/polymer	E_m^p (V)	ΔE (V)	E_g^{OPT} (eV)	HOMO (eV)	LUMO (eV)
FT2F	0.80; −1.45[a]	2.25	2.31	5.53	3.28
c-H2T2FT2	0.70; −1.45[a]	2.15	2.09	5.43	3.28
T2F	0,75; −1.6	2.35	2.38	5.48	3.13
H4FT6F[32]	0.22, 052; −1.68	1.90	1.96	4.95	3.05
TFT	0.95; −1.42[a]	2.37	2.34	5.68	3.31
H2TFT	0.99; −1.50[a]	2.49	2.41	5.72	3.23
T2FT2	050, 080; −1.65[b]	2.15	2.19	5.23	3.08
H4T3FT3	0.66; −1.47[a]	2.13	2.10	5.39	3.26
poly(TFT)[a]	0.8; −1.6	2.4	2.08	5.53	3.13
poly(H2TFT)[a]	0.95; −1.53	2.48	2.18 2.35[b]	5.68	3.20
poly(T2FT2)[a]	0.8; −1.65	2.45	1.85	5.53	3.08
poly(H4T3FT3)[a]	0.6; −1.6	2.20	1.91	5.33	3.13

[a] E^0 is the average of forward and backward peak potentials; conditions for electrochemistry are given in the text. [b] Chlorobenzene solution.

at a potential close to that of **FT2F**. If a thienyl ring terminates the molecular backbone, the radical cation will couple at the free 5-position, giving dimers (if only one 2-thienyl residue terminates the molecule) or polymers (two 2-thienyl end-groups).

The **T2F** molecule is expected to undertake a dimerisation to yield **FT4F**, not considered in Scheme 1 because it is completely insoluble. In fact, the CV of **T2F** indicates irreversible oxidation at 0.75 V, with dimer formation, and reversible reduction at −1.6 V.

The electrochemical dimerization of **H2T3F** to give **H4FT6F** and the electrochemistry together with other chemical characterizations (^{1}H-NMR, FTIR, UV-Vis spectroscopy, MALDI, elemental analysis) of the latter have been reported in ref. 32.

The CV traces of **H2TFT**, **TFT**, **T2FT2**, and **H4T3FT3** monomers (not shown) indicate an irreversible oxidation process for anodic coupling at peak potentials of 0.99, 0.95, 0.66 and 0.66 V respectively. The absence of any lowering of the oxidation potential for the longest oligomer can be accounted for by the presence of the hexyl chains on the inner thiophene ring producing a twisting of the arms of the molecule, as described in ref. 36.

Fig. 1 presents the cyclic voltammograms of the polymers obtained from **TFT**, **H2TFT**, **T2FT2**, and **H4T3FT3**. The oxidation of the considered polymers is anodically shifted to *ca.* 0.8, 0.95, 0.5 and 0.3 V respectively. Thus the trend of lower oxidation potential with longer **T** chains is retained in the polymer, with an additional reduction by 0.15–0.3 V from the potential of polymerization. In **poly(H2TFT)**, this additional reduction does not exceed 0.05 V due to its only slight gain in conjugation, while in poly(FDOBT),[37] obtained from the corresponding oligomer with the alkyl substitution on 4-position of thiophene ring, this additional reduction is maintained (see ESI†). **Poly(H4T3FT3)** shows the largest shift of oxidation potential, which can be related to a planarization of the 3′,4′-dihexyl-2:2′;5′:2″-terthiophene residue in the polymer with respect to **H4T3FT3** molecule, due to the blocking of the terminal **T** rings.

The CVs of all compounds in acetonitrile show a reversible one-electron reduction process due to the fluorenonyl moiety. The redox potential at *ca.* −1.45 V in the monomers is cathodically shifted to −1.60 V in the polymers, as a result of the electron donor properties of the oligothiophene moieties in the backbone. The specific electrochemistry of each molecule to give polymers is reported in the ESI,† together with the FTIR characterization of the polymers, which indicates an high degree of polymerization reached by electrosynthesis.

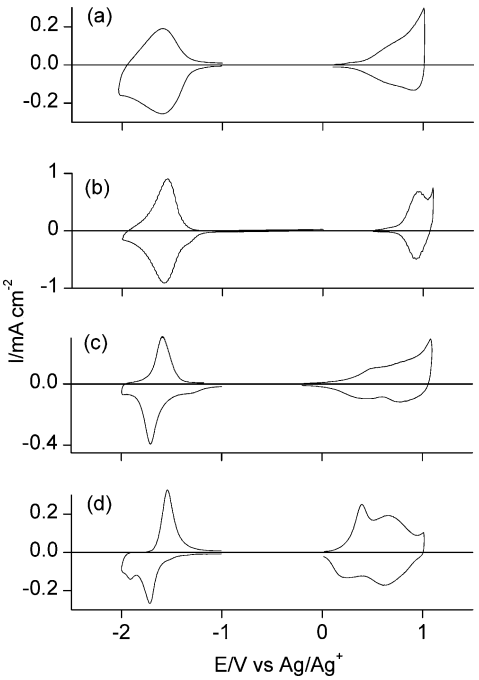

Fig. 1 Cyclic voltammogram of (a) poly(TFT); (b) poly(H2TFT); (c) poly(T2FT2) and (d) poly(H4T3FT3) in acetonitrile + 0.1 M Bu_4NClO_4. Scan rate: 0.1 V s^{-1}.

2.3 Optical characterization of monomers and polymers

In the compounds studied, appropriate setting up of units and side chains allows for direct control of the energy gap (E_g); in fact, the optical absorption can be tuned by modulating the planarity of these compounds. The electronic absorption spectra of oligomers in the solid-state and solution ($CHCl_3$ or chlorobenzene depending on their solubility), shown in Fig. 2, display characteristic absorption bands, namely a more intense absorption maximum and a shoulder. The high energy peak is attributable to transitions from the thiophene-based valence band to its antibonding counterpart. The weaker band, often a shoulder, in the visible range (480–650 nm) has been extensively discussed in literature and is attributable to the n–π* transition in the carbonyl group of the **F** unit,[1,4] or to an internal charge transfer band (ICT) due to the combination of the electron-donating thiophene blocks with an electron-withdrawing **F** central unit.[12] In addition, unsubstituted molecules and those with only two end-chains display at higher energy a further excitonic band, indicating the formation of H aggregates even at concentration of 10^{-4}–10^{-5} M. In contrast, the presence of the band due to the π–π* transition of the isolated molecule in spin-coated films is attributable to the disordered regions, and for this reason OFET device films are deposited by vacuum evaporation. Due to the presence of an indium thin oxide layer on a glass substrate, the profiles of absorption spectra of some monomer films (**FT2F**, **H4FT6F**, **H4T3FT3**) rise and those of all polymer films are cut off at around 300 nm.

For molecules with four alkyl chains **H4T3FT3** and **H4FT6F**, the expected bathochromic shift of the absorption spectrum appears on going from solution to the solid state (bottom of Fig. 2a and b); moreover, the spectrum of the latter extends even into the visible part of the solar spectrum, indicating that they could be candidates for photovoltaic (PV) applications (see below).[12]

The E_g values for the monomers were evaluated from the electrochemical gaps (ΔE) and from optical data of the solution regarding the spectra band edge (E_g^{OPT}). A comparison between these two sets of data reported in Table 1 provides evidence for a substantial agreement.

 This journal is © The Royal Society of Chemistry and the Centre National de la Recherche Scientifique 2010

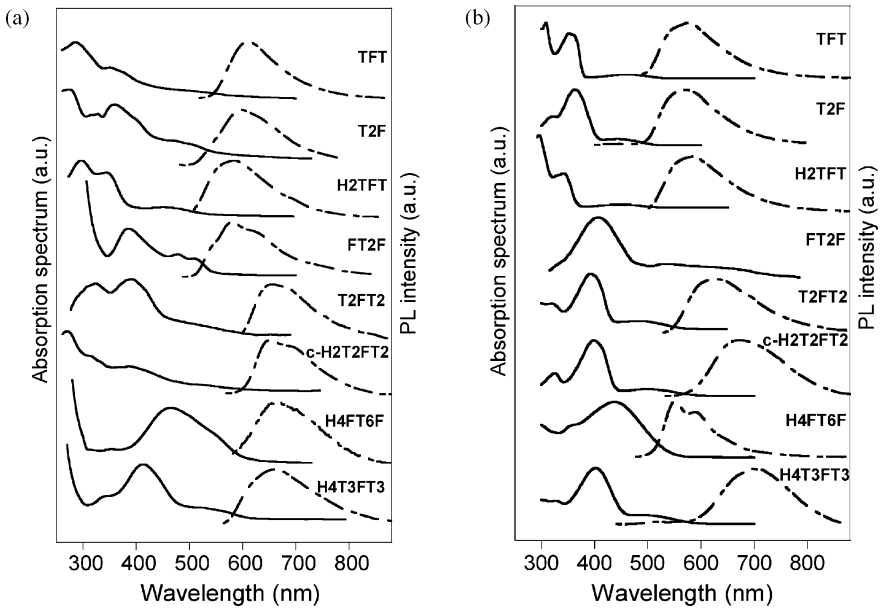

Fig. 2 Absorption (solid lines) and PL spectra (dashed lines) in solid-state (a) and solution (chloroform or chlorobenzene) of the molecules (b).

The PL spectra of molecules in solution and as spin-coated films from chlorobenzene solutions (vacuum-sublimated in the case of the insoluble **T2FT2** and **FT2F**) are also shown in Fig. 2. The PL quantum yield (QY) is rather low even in solution – 10% for **TFT** in THF and lower for all the other compounds. This is attributable both to the presence of **F** residue, which is low-emitting by itself, and to concentration quenching effects occurring once **F** and **T** units can interact electronically.[6] The PLQY of films decreases further, which can likely be ascribed to the packing tendency of the oligomers through their π–π and CT interactions. Substitution with hexyl chains affects the PLQY, depending both on their number and position and on the thiophene position in the oligomer sequence. The distortion of adjacent thiophene rings, due to hexyl chains in the 3- or 4-positions, leads to a solid-state PLQY of 3% for **H2TFT** compound (the highest among the investigated compounds), while the backbone planarity, as in **T2FT2**, **FT2F**, and **c-H2T2FT2** (chains in the 5-position), causes almost complete quenching of the emission. Details on peak position for absorption and emission spectra are reported in the ESI†.

The absorption spectra of the polymer films, reported in Fig. 3, show the same features of the corresponding monomer in the case of **poly(H2TFT)**, while the spectra are shifted towards longer wavelengths for **poly(TFT)**, **poly(T2FT2)** and **poly(H4T3FT3)** due to increased planarization of thiophene segments.

Only in the unique case of a soluble polymer, *i.e.* **poly(H2TFT)**, is the E_g^{OPT} from the optical band edge of the solution spectrum close to the electrochemical one, while for other polymers the difference is significantly larger.

Due to the increasing number of interconnections in the polymeric films, a further strong decrease of the PLQY occurs with respect to the corresponding monomers, and the hence emission intensity is not detectable by the apparatus.

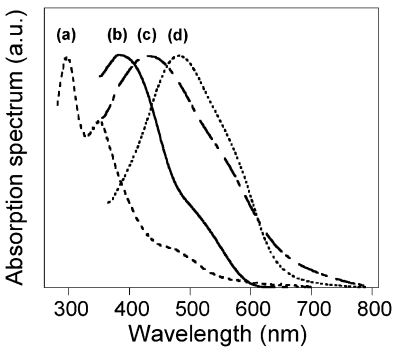

Fig. 3 Absorption spectra of **poly(H2TFT)** (a), **poly(TFT)** (b), **poly(T2FT2)** (c) and **poly(H4T3FT3)** films (d).

The PL maximum for **poly(H4T3FT3)** and **poly(TFT)** is the same (λ_{max} at *ca.* 675 nm), independent of the number of thiophene rings, whereas it is blue-shifted for **poly(H2TFT)** (peak at 600 nm) due to the steric hindrance of the substitution pattern.

2.4 DFT calculations

Ab initio calculations, especially in the frame of DFT, are useful in determining electronic properties; as a matter of fact, recent studies on **F**-based oligomers, as well as a series of oligomers based on 3,4-phenylenedioxythiophene, have been reported.[4,19,30,38] We adopted similar procedures, in order to shed light on chemical stability and extent of delocalization, and to compare it with electrochemical and spectroscopic data. The four molecules investigated, namely **TFT**, **T2F**, **T2FT2** and **FT2F**, represent typical alternation of D and A moieties.[28]

Calculations were carried out using the B3LYP hybrid density functional: we tried various basis sets, starting from a plain 3-21G, up to 6-311G-supplemented with polarization functions and diffuse function on electronegative atoms (S and O).

Geometries in agreement with X-ray data were used as a starting point for energy minimizations; the latter were carried out in vacuum. Constrained geometries were also tested, in order to ensure that the backbone remained essentially planar. In Table 2, the results of calculations of the differences between the highest occupied molecular orbital (HOMO) and the lowest unoccupied molecular orbital (LUMO) are reported and compared with E_g^{OPT} values in both film and solution, since the calculations refer to an isolated molecule, while device performances are obviously determined on thin films. We found the the values of both series show a trend fully consistent with both the electrochemical and optical investigations. In Fig. 4, the HOMO and LUMO orbitals for the four molecules are shown.

It is evident that for the **TFT** the HOMO density is equally distributed all along the molecule (Fig. 4a), as is also observable for **T2FT2** (Fig. 4e), while for **T2F** (Fig. 4c) the density is essentially confined onto the **T** residues. On the other hand, in **FT2F** (Fig. 4g) the electronic density is more concentrated on the inner part. As expected, the LUMO orbitals follow a different trend, namely that the **F** moiety has high electron density in all the cases (Fig. 4b, d, f and h), only in **FT2F** does the **T** segment display some electron density.

Table 2 (HOMO − LUMO) energy differences (eV) as computed at various level of theory with the B3LYP hybrid functional[a]

	FT2F	T2FT2	T2F	TFT
Experimental values (on oligomers)				
$E_{g,obs}$ film solution	2.25	2.19	2.38	2.34
$E_{g,calc}$	2.85	2.80	3.02	3.22
Calculated values (on monomers)				
3-21G	2.77	2.84	3.05	3.04
3-21G* F	2.88	2.77	3.04	3.16
3-21G* solv	2.77	2.75	2.97	3.11
6-31G** F	2.80	2.69	2.94	3.07
6-31G** solv	2.69	2.68	2.88	3.01
6-311G**+ F	2.72	2.69	—	—
6-311G**+ +	2.73	2.65	—	—

[a] Calculations were performed on an isolated molecule, hence the E_g value to compare with is the one measured in solution. Addition of the diffuse functions (+) on S and O atoms does not reflect systematically on the results; neither does freezing all dihedrals (**F**) to planarity.

Noticeably, both HOMO and LUMO electron density contours are consistently comparable with those of the **F**-containing oligomers reported in ref. 9 and 38. Moreover, the CV results (see above) completely agree with the reported observations, *i.e.* the electron density contours map the ease of

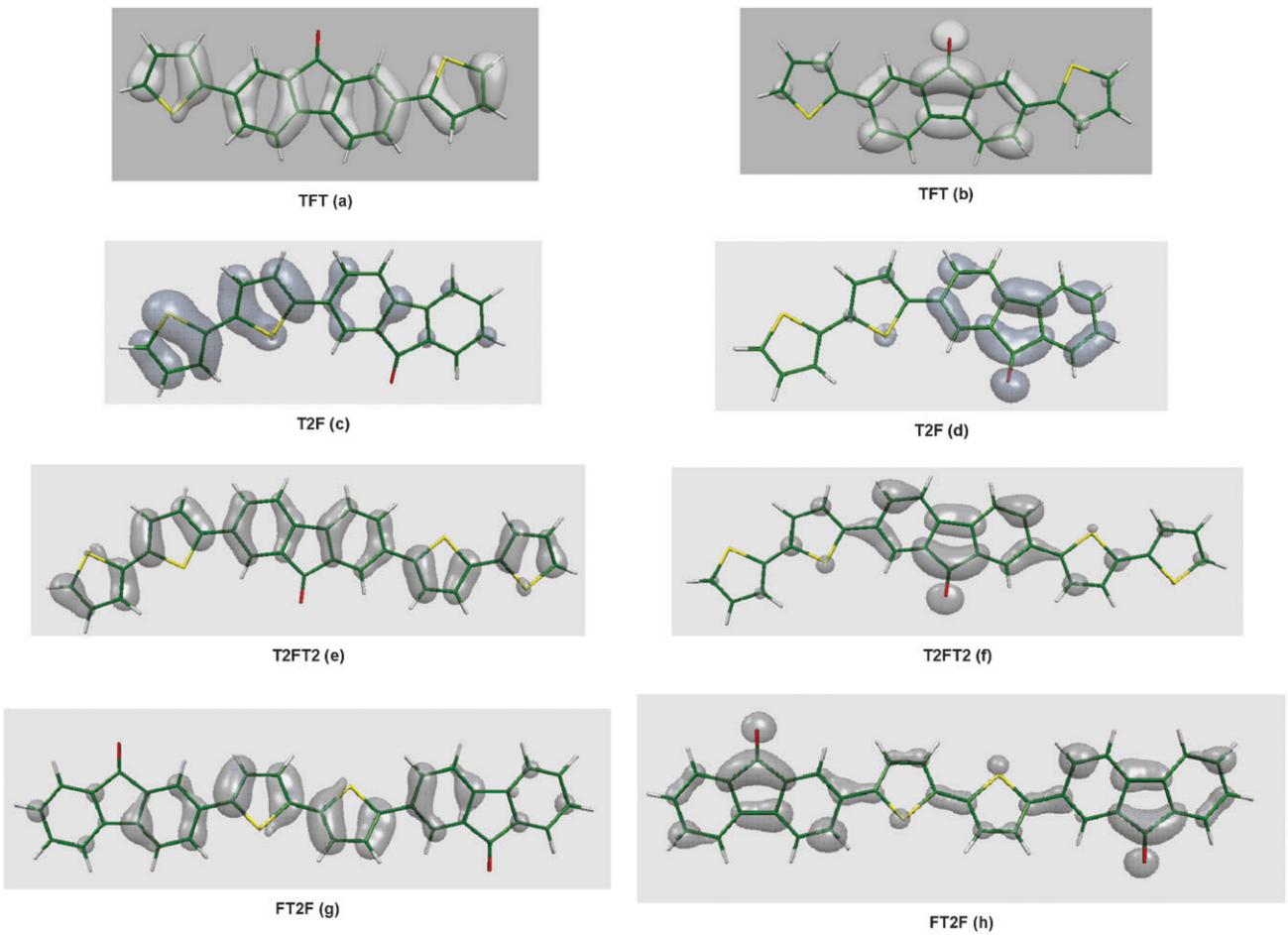

Fig. 4 HOMO and LUMO orbitals (cut-off at 0.025 H) for the molecules **TFT** (a) and (b), **T2F** (c) and (d), **T2FT2** (e) and (f), **FT2F** (g) and (h) respectively. Only parts with positive value are shown for clarity, in transparent mode.

 This journal is © The Royal Society of Chemistry and the Centre National de la Recherche Scientifique 2010

radical formation and subsequent evolution. In this view, **TFT** and **T2FT2** oligomers undergo polymerization, while **T2F** evolves into dimer **FT4F**; in contrast, **FT2F** is stable towards oxidation.

2.5 Structural and morphological characterizations

Understanding the solid-state arrangement is necessary to investigate the structure/orientation of molecules in thin films of devices. In particular, packing closeness can be checked due to knowledge of the unit cell parameters allowing one to perform **PF** calculations reliably.[25] XRD crystal structures of selected molecules were investigated as single crystals (**TFT**) or as powders (**FT2F**, **c-H2T2FT2**, **H4FT6F**).[13,14,26,36] All display close packing, thanks to the strong fluorenone-H interactions (see packing reported in Fig. 5). For the molecules for which the structure was not solved, detailed molecular modelling calculations using Material Studio package[39] were carried out and combined with XRD on thin films, reliably indicating the molecular orientation in the active layers of prototype of devices.

It is worth comparing the packing of **TFT**, **FT2F**, **c-H2T2FT2** oligomers (Fig. 5) with that of 2,7-bis(4-(*tert*-butylthio)phenyl)fluorenone crystal (DSFO),[19] where the formation of H-bonds clearly induces the dimer packing, and hence the excimer formation, resulting in its notable emission properties.

In **TFT** crystals (see ORTEP view in ESI†) the molecules pack in pairs linked by H-bonds (0.245 nm); other contacts involving H (S–H, 0.271 nm) between adjacent pairs complete the close packing, recalling that of DSFO (H-bond 0.254 nm). However, in DSFO the other interactions connecting dimers are clearly looser, in fact the density is lower (1.24 g cm^{-3} *versus* 1.45 g cm^{-3}). Therefore, in DSFO excimer formation favors emission, while in **TFT**, due to large PF value ($\sim$0.73) the luminescence is largely quenched.

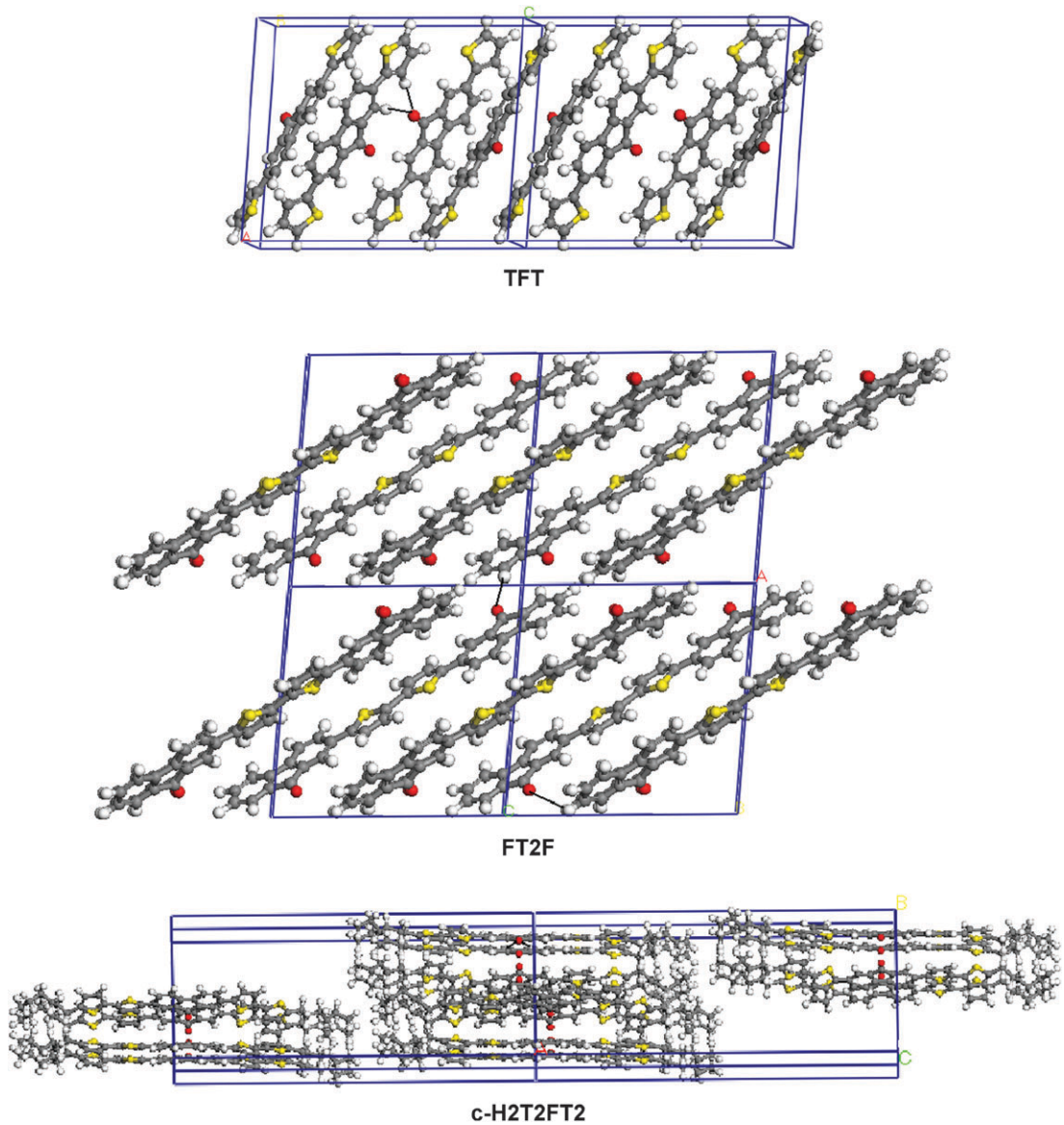

Fig. 5 Crystal packing of **TFT**, **FT2F**, and **c-H2T2FT2** oligomers. The black line indicates H-interactions involving the carboxyl moiety.

A different situation occurs in the crystal structure of **FT2F**, where strong H-interactions are present (0.26 nm), but where dimer formation is not observed. The packing can be described as two inverse sequences of single molecules essentially overlapping along the short *a* axis.

Similar packing is found in **c-H2T2FT2**, where an alternating sequence of molecules interact by short H-bonds (0.235–0.241 nm), along the short *c* axis; however, the other contacts are a bit looser, approaching the sum of the Van der Waals radii.

In spite of the close packing observed, none of the structures investigated support the excimer formation being different from that for crystals of DSFO,[19] fully justifying the observed poor emission properties (see optical characterization).

Thin-film arrangements were next studied directly in the device prototypes. Fig. 6 reports the XRD spectrum of film into OFET device of six typical molecules: **TFT**, **T2F**, and **T2FT2** (Fig. 6a) and **H4T3FT3**, **c-H2T2FT2**, and **FT2F** (Fig. 6b). The experimental film thicknesses range from 25 nm to 100 nm.

Detailed analyses of the profiles give the following relevant information:

– in the **TFT** spectrum, four [100] directions are detected, the one at largest 2θ° being attributed to the substrate.

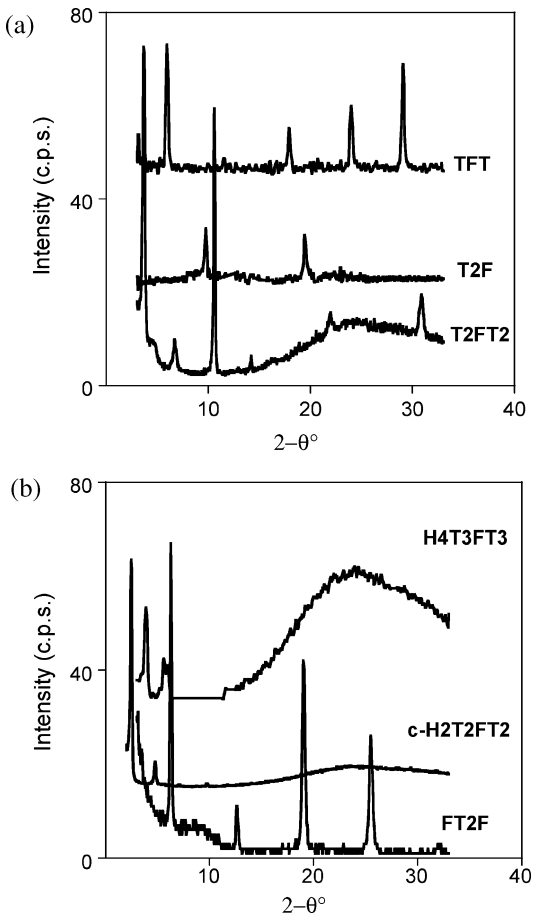

Fig. 6 XRD patterns of oligomer films, with the thickness in parenthesis: (a) top **TFT** (30 nm), middle **T2F** (42 nm), and bottom **T2FT2** (100 nm); (b) top **H4T3FT3** (25 nm), middle **c-H2T2FT2** (40 nm), and bottom **FT2F** (50 nm). The intensities are slightly shifted for clarity.

Table 3 Molecular orientation of selected oligomers from coupling of XRD analysis and molecular modelling (MM)[a]

Oligomer	Orientation direction	α [b]
TFT	[100]	64°
T2F	Medium axis [c]	30° [d]
T2FT2	[100] [c]	60° [d]
H4T3FT3	Three orientations	All <30°
c-H2T2FT2	[100] [b]	~90°
FT2F	[100] + others [c]	All <45°
H4FT6F	Single [f]	~90°

[a] For details see text. [b] The angle is formed by molecular axis and the substrate plane. [c] More orders of the same crystallographic direction, *i.e.* unique orientation along the axis. [d] The value is similar in case of card-pack or herringbone arrangements. [e] The three observed peaks result from the overlap of more directions, as detailed in ref. 26. [f] The unique orientation is detailed in ref. 36.

– in the **T2F** spectrum, two medium axis directions (0.91 nm) are detected.

– in the **T2FT2** case, up to eight long axis directions (4.4 nm) are observable.

– in the **H4T3FT3** film, three non-commensurate peaks are detected, *i.e.* three different orientations.

– in the **c-H2T2FT2** film, two [100] directions are observed.[14]

– in the **FT2F** film, four peaks are detected, the [100] direction being prevalent, and the remaining three being sums of other crystallographic directions[26] (2–4 reflections), namely [001], [202], and [113].[26]

By combining XRD analysis with molecular modeling,[39] approximate angles between molecular axis and orientations direction can be derived, and the results are summarized in Table 3. As a result, in both the case of card-pack (**TFT**) and herringbone arrangements (**c-H2T2FT2**), shown in Fig. 5, the angle between the molecular axis and the substrate plane (α) is crucial to understand the electrical properties.

For the **T2FT2** molecule, whatever structural motif is adopted the α value is over 60°, whereas for the **T2F** oligomer the value is close to 30°. A particular case is presented by **FT2F** molecule, whose XRD pattern displays peaks comprising the combination of different reflections, irrespective of the kind of deposition adopted (*e.g.* high-vacuum evaporation or spin-coating), implying multiple molecular orientations in the films.[26] However, in all the orientations, except for [001], for which the weight is ~0.12, the α value ranges from 15° to 30°. **H4T3FT3** adopts three different orientations, likely due to the position of the alkyl chains. As the length of the molecule's conjugated backbone is close to 3.0 nm, the orientation of the molecular axis perpendicular to the surface has to be ruled out.

In summary, when the molecule comprises a sequence of **F** and **T** residues without substituents, the molecular orientation is approximately edge-on, *i.e.* the average molecular axis forms with the substrate plane an angle greater than 60°, unless the molecule is asymmetric and relatively short (**T2F**). In contrast, when alkyl chains are present, the situation is modified according to the substitution site; namely, if the chains are end-capping the molecule, the orientation is again edge-on, while substitution at the 3,4-positions of the thiophene rings implies a multiple orientation that is partly edge-on, with the

 This journal is © The Royal Society of Chemistry and the Centre National de la Recherche Scientifique 2010

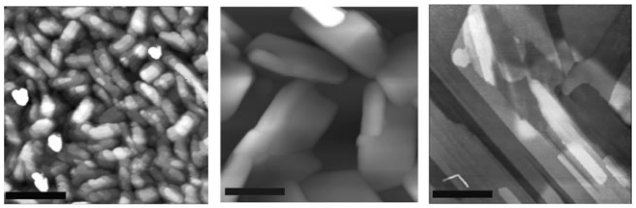

Fig. 7 AFM height images of OFET devices of: (a) **T2FT2**, (b) **T2F**, and (c) **c-H2T2FT2** in tapping mode; only height images are shown for clarity. The black bar in (a) corresponds to 500 nm for all the three images. The measured roughnesses are 20 nm, 130 nm, and 10 nm respectively.

alkyl chains pointing alternately upwards or towards the substrate.

Finally, the semi-crystalline **H4FT6F** adopts an approximate edge-on orientation of the backbone with side-chains separating adjacent molecules, yielding relatively loose packing.[36]

AFM investigations into OFET devices based on three typical molecules are reported here as examples in order to verify the crystal interconnections. In Fig. 7 three topographic images of **T2FT2**, **T2F**, and **c-H2T2FT2** films (thickness 40–50 nm) obtained by high-vacuum evaporation, are shown for comparison. The roughness as well as the interconnections among crystals are different in the three cases:

– in the **T2FT2** device, efficient interconnection is detected (Fig. 7a).

– in the **T2F** film, some voids are evident due to a larger aggregate size (Fig. 7b).

– in the optimised layer **c-H2T2FT2**,[14] the interconnection is guaranteed and the roughness is strongly reduced (Fig. 7c).

These observations are in agreement with OFET device results (see below).

2.6 Potential applications

2.6.1 OFET device measurements. Many of the reported molecules were next tested as active layers in p-type devices, with the aim of putting forward a relation between chemical constitution and performance of un-optimized devices. In Table 4 relevant results from molecules displaying closest packing are presented. The mobility and $I_{on/off}$ values were derived from output characteristic *I–V* curves reported in the ESI†, according to the procedure described in the Experimental section and in ref. 14.

The generally low values of both mobility and $I_{on/off}$ ratios can be accounted for by coupling the surface/structural investigations with electrochemical and optical data, and DFT calculations. In fact, the best value of the OFET performances in p-type devices is achieved in the case of a stable molecule, well oriented with respect to the electrode and with compact morphology (**c-H2T2FT2**), while the worst results are found in the case of the well oriented but **T**-terminated molecule (irreversible oxidation process) (**TFT**), or in the case of molecular multiple orientations (**FT2F**); while intermediate values are reached in case of incomplete substrate coverage (**T2F**), *i.e.* bad crystal interconnections. Hence the crucial effects dominating the FET functioning are definitely mapped. In the light of the above results, the approach followed by Curtis,[28] *i.e.* D and A parts in the molecule, seems to be rather restrictive for deciding which compounds to choose for FET applications; in fact, the possibility of oxidation, the packing interactions, and the substrate influence contribute to determine the appropriate choice. Indeed, a recent review by Roncali[29] strongly supports this observation.

Table 4 Electrical measurements of p-type OFET devices based on **F**-molecules

Oligomer	μ ($cm^2\ V^{-1}\ s^{-1}$)	$I_{on/off}$	Ref.
TFT	$\leq 10^{-7}$	<10	15
FT2F	$\leq 10^{-7}$	<10	15
T2F	2×10^{-6}	$<10^2$	Present work
T2FT2	5×10^{-4}	$>10^3$	Present work
c-H2T2FT2	$>2 \times 10^{-3}$	7×10^5	24
H4FT6F	7×10^{-5}	≤ 30	36

2.6.2 Solar cell evaluation. The potential use of the compounds studied in BHJ solar cells deserves careful evaluation of their electronic levels. In fact, choosing the typical acceptor [6,6]-phenyl-C_{61}-butyric acid methyl ester (PCBM),[40] in principle all could be considered as candidates because their HOMO level values range from 4.95 eV to 5.72 eV (for **H4FT6F** and **H2TFT** respectively). However, their harvesting capability (see absorption spectra above), coupled with their processability, limits the choice of compounds to either **H4T3FT3** or **H4FT6F**, provided that the compatibility of blends with PCBM or other acceptor molecules allows for homogeneous film fabrication. As the latter molecule better fits such a requirement, BHJ devices based on **H4FT6F** were tested with PCBM in a 1:1 ratio by weight (see the Experimental section for details). For a series of un-optimized devices, the results reported in Table 5 were obtained, *i.e.* a power conversion efficiency close to 0.8% was achieved. Comparison with Demadrille's results[12] concerning a series of **T**- and **F**-containing oligomers reveals that long $\mathbf{T}_n$ sequence molecules display the best performances. The *I–V* curve together with absorption spectrum of the device is presented in Fig. 8.

3. Conclusions

A careful study has been performed on fluorenone-containing oligomers, designed to achieve an effect on the electronic and optical properties from alternating **T** and **F** residues and the presence and position of alkyl chains. The electrochemical data, which are in agreement with optical characterizations, have been corroborated by DFT calculations on four

Table 5 Photovoltaic properties of **H4FT6F** molecule/PCBM-based devices. Measurement under AM 1.5 at 100 mW cm^{-2}). V_{OC}: open circuit voltage, FF: fill factor, J_{SC}: short-circuit, η: power conversion efficiency

Sample[a]	V_{oc} (V)	FF	J_{sc} (mA cm^{-2})	η (%)
A, 1000 rpm	0.74	0.34	2.95	0.72
B, 1000 rpm	0.74	0.34	2.92	0.73
A, 1500 rpm	0.64	0.29	3.05	0.67
B, 1500 rpm	0.70	0.37	3.03	0.77

[a] The values are averaged; the e.s.d. is 0.03.

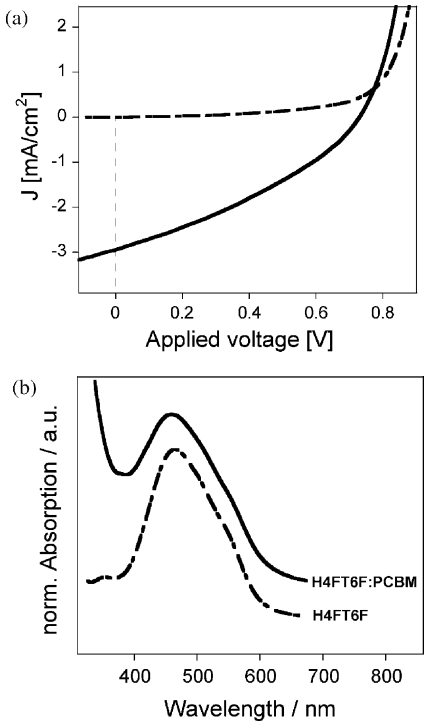

Fig. 8 *J–V* curve of the BHJ device: (a) in the dark (dotted line) and upon AM1.5 irradiation (solid line). Normalized absorption spectrum (b) of the **H4FT6F** film (dotted line) and of the device (solid line). Spectra are shifted for clarity.

examples. These also afforded orbital maps that enabled us to understand both the chemical stability and the behaviour in FET devices. Structural analyses, fully in agreement with the other characterisation data, were carried out on single crystals and powders, allowing for the determination of molecular orientations in thin films. The findings clearly explain the performances in OFETs, taking into account the effective close-packing induced by fluorenone. In addition, some chemical structure markers enabling us to identify structures suitable for FET or solar cell fabrication have been pinpointed. Namely, alkyl substitution on the thiophene rings, which enables processability, only results in close-packing if placed at the 2- and 5-positions (end chains), while positioning the fluorenone at the end of an oligomer permits reversible oxidation. Finally, long **T**-sequences only can supply adequate light harvesting by extending absorption towards the red region.

In summary, the **F** residue, when inserted as end-capper in the oligomers, results in close-packing formation and chemical stability.

4. Experimental section

4.1 Chemicals and reagents

All melting points are uncorrected. All reactions of air- or water-sensitive materials were performed under nitrogen. Air- and water-sensitive solutions were transferred with double-ended needles (cannulas). The solvents used in the reactions – THF (Fluka) and toluene (Aldrich) – were dried and stored over molecular sieves. Acetonitrile was reagent grade (Uvasol, Merck) with a water content $<0.01\%$. The supporting electrolyte tetrabutylammonium perchlorate (Bu_4NClO_4), methylene chloride and chlorobenzene were reagent grade and used as received. Butyllithium (BuLi), bromohexane, 2-isopropoxy-(4,4,5,5-tetramethyl)-1,3,2-dioxoborolane, 2-bromo-9-fluorenone, 2,7-dibromo-9-fluorenone, 2,2′-bithiophene-5-boronic acid pinacol ester, and 2-(tributylstannyl)thiophene), *N*-bromosuccinimide (NBS) and tetrakis-(triphenylphosphine)palladium [$(Ph_3P)_4Pd$] available from Aldrich, were used as received, while bithiophene and 3-bromothiophene were purified by flash chromatography and distillation respectively. 5-(4,4,5,5-Tetramethyl-1,3,2-dioxaborolan-2-yl)-3′-4′-dihexyl-2,2′:5′,2″-terthiophene and 3-hexylthiophene-2-boronic acid pinacol ester and were prepared according to ref. 32 and 41 respectively. Flash chromatography was carried out using silica gel (200–300 mesh ASTM). Suzuki reactions were carried out with conventional heating.

4.2 Syntheses

4.2.1 2,7-Bis(3-hexylthien-2-yl)fluoren-9-one (H2TFT). In a 25 mL Schlenk tube was introduced 213 mg (0.73 mmol) of 3-hexylthiophene-2-boronic acid pinacol ester, 122 mg (0.36 mmol) of 2,7-dibromo-9-fluorenone and 21 mg of $(Ph_3P)_4Pd$. Then, 4 mL of anhydrous THF and 2.5 mL 2 M K_2CO_3 were added to this mixture under nitrogen. The reaction was stirred at reflux overnight, and the resulting orange-brown oil isolated by extraction with dichloromethane (CH_2Cl_2) (3 × 100 ml). The combined organic layer was dried over anhydrous magnesium sulfate, and the solvent removed by rotary evaporation, giving a powder which was subjected to purification by flash chromatography using silica gel with hexane–ethyl acetate 9:1 as eluent, to give 128 mg of pure product (70% yield). MS (gas-phase) m/z 511 (M^+). ^{1}H NMR (270 MHz, $CDCl_3$ δ_H/ppm, 25 °C): 7.74 (s, 2H, fluorenyl), 7.56 (br, 4H, fluorenyl), 7.25 (d, J = 5.20 Hz, 2H, thienyl), 6.99 (d, J = 5.20 Hz, 2H, thienyl), 2.67 (t, 4H, J = 7.61, alkyl chain), 1.62 (m, 4H, alkyl chain), 1.29–1.20 (br, 12H, alkyl chain), 0.85 (m, 6H, alkyl chain). M.p. = 277 °C. Elemental analysis: Calc. for $C_{33}S_2O_1H_{36}$: C, 77.34; S, 12.51; O, 3.12; H, 7.03. Found: C, 77.41; S, 12.43; H, 7.19.

4.2.2 2-(2,2′-Bithiophene-5-yl)fluoren-9-one (T2F). In a 25 ml Schlenk tube was introduced 226 mg (0.77 mmol) of 2,2′-bithiophene-5-boronic acid pinacol ester, 128 mg (0.50 mmol) of 2-bromo-9-fluorenone and 10 mg of $(Ph_3P)_4Pd$. Then, 4 ml of distilled THF and 2.5 ml 2 M K_2CO_3 were added to this mixture under nitrogen. The reaction was stirred at reflux overnight, the mixture poured into water and extracted with dichloromethane (CH_2Cl_2) (3 × 100 ml). The combined organic layer was dried over anhydrous magnesium sulfate, and the solvent removed by rotary evaporator, giving a powder which was subjected to purification by flash chromatography using silica gel with hexane–ethyl acetate 8:2 as eluent, to obtain 117 mg of pure product (68% yield). MS (gas-phase) m/z 343 (M^+). ^{1}H NMR (270 MHz, $CDCl_3$ δ_H/ppm, 25 °C): 7.89 (s, 1H, fluorenyl), 7.71–7.67 (br, 2H, fluorenyl), 7.53–748 (br, 3H, fluorenyl), 7.32–7.28 (br, 2H, 1H thienyl + 1H fluorenyl), 7.25 (d, J = 5.81 Hz, 1H, thienyl), 7.22

 This journal is © The Royal Society of Chemistry and the Centre National de la Recherche Scientifique 2010

(d, J = 3.58 Hz, 1H, thienyl), 7.17 (d, J = 3.58 Hz, 1H, thienyl), 7.045 (dd, J = 5.81 Hz, J = 3.90 Hz, 1H, thienyl). Elemental analysis: Calc. for $C_{21}S_2O_1H_{12}$: C, 73.25; S, 18.60; O, 4.65; H, 3.49. Found: C, 73.41; S, 18.56; H, 3.52.

4.2.3 2,7-Bis(3′,4′-Dihexyl-2,2′:5′,2″-terthiophene-5-yl)-fluoren-9-one (H4T3FT3). To a Schlenk tube containing 0.57 mmol of 5-(4,4,5,5-tetramethyl-1,3,2-dioxaborolan-2-yl)-3′-4′-dihexyl-2,2′:5′,2″-terthiophene in THF solution (4.5 mL) was added 1 mL of a 2 M solution of K_2CO_3 in degassed water, and the mixture was stirred for 1 h. Separately, a solution of 54 mg (0.16 mmol) of 2,7-dibromofluorenone in 1.5 mL of distilled tetrahydrofuran (THF) was transferred *via* cannula to the flask containing the borolane derivative. After the addition of a catalytic amount of $(Ph_3P)_4Pd$ (11 mg), the reaction temperature was increased to 70 °C, the mixture refluxed overnight with stirring, then quenched with acid water and dried over magnesium sulfate. The solvent was removed and the residue was purified by flash column chromatography, using hexane–dichloromethane 7:3 as eluent, to provide 49 mg of title product as a red-brown solid (55% yield). MS (MALDI): m/z 1009 ^{1}H NMR (270 MHz, $CDCl_3$, δ_H/ppm, 25 °C): 7.86 (d, 1H, J = 1.5 Hz, fluorenyl), 7.66 (dd, 1H, $J_{3,1}$ = 1.5 Hz, $J_{3,4}$ = 7.8 Hz, fluorenyl), 7.46 (d, 1H, $J_{4,3}$ = 7.8 Hz, fluorenyl), 7.29–7.32 (m, 2H, thienyl), 7.09 (d, 1H, J = 3.77 Hz, thienyl), 7.14 (m, 1H, thienyl), 7.06 (m, 1H, thienyl), 2.67–2.75 (m, 4H, alkyl chain), 1.53–1.59 (m, 4H, alkyl chain), 1.32–1.47 (br, 12H, alkyl chain), 0.92 (m, 6H, alkyl chain). Elemental analysis: Calc. for $C_{61}S_6O_1H_{68}$: C, 72.63; S, 19.04; O, 1.59; H, 6.74. Found: C, 72.97; S, 18.84; H, 6.81.

4.2.4 2,7-Bis(2,2′-Bithiophene-5′-yl)fluoren-9-one (T2FT2). In a 25 mL Schlenk tube, 263 mg (0.9 mmol) of 2,2′-bithiophene-5-boronic acid pinacol ester, 128 mg (0.38 mmol) of 2,7-bromo-9-fluorenone and 20 mg of $(Ph_3P)_4Pd$ were introduced. Then, 4 mL of distilled THF and 2.5 mL 2 M K_2CO_3 were added to this mixture under nitrogen. The reaction was stirred at reflux overnight, and the mixture poured into water and extracted with dichloromethane (CH_2Cl_2) (3 × 100 mL). The combined organic layer was dried over anhydrous magnesium sulfate, and the solvent removed by rotary evaporator, giving a red powder. MS (gas-phase) m/z 508 (M^+). ^{1}H NMR (270 MHz, d_8-dimethyl formamide, δ_H/ppm, 120 °C): 7.93–7.90 (m, 2H, fluorenyl), 7.85 (d, 1H, J = 7.4 Hz, fluorenyl), 7.58 (d, 1H, J = 3.82 Hz, thienyl), 7.49 (dd, 1H, $J_{4,3}$ = 3.59 Hz, $J_{3,5}$ = 1.08 Hz thienyl), 7.38 (1H, dd, $J_{5,4}$ = 5.1 Hz, $J_{3,5}$ = 1.04 Hz, thienyl), 7.32 (d, 1H, J = 3.82 Hz, thienyl), 7.12 (dd, 1H, $J_{3,4}$ = 3.72 Hz, $J_{4,5}$ = 5.0 Hz, thienyl). Mass fragmentation and ^{1}H NMR spectra are reported in the ESI†. Elemental analysis: Calc. for $C_{29}S_4O_1H_{16}$: C, 68.51; S, 25.17; H, 3.16. Found: C, 68.80; S, 24.87; H, 3.05.

4.3 Apparatus and procedures

4.3.1 General electrochemistry. The compounds were generally investigated in acetonitrile + 0.1 M Bu_4NClO_4 (conc. $\sim 10^{-3}$ M). Methylene chloride and chlorobenzene were used for **H4T3FT3** and **T2FT2** respectively for solubility reasons. Electrodeposited films were in all cases investigated in acetonitrile + 0.1 M Bu_4NClO_4.

Electrochemical experiments were performed at room temperature under nitrogen in three-electrode cells. The counter-electrode was platinum; the reference electrode was silver//0.1 M silver perchlorate in acetonitrile (0.34 V *vs.* SCE). The voltammetric apparatus (AMEL, Italy) included a 551 potentiostat modulated by a 568 programmable function generator and coupled to a 731 digital integrator. The working electrode for cyclic voltammetry was a platinum minidisc electrode (0.003 cm^2). For electronic spectroscopy, a 0.8 × 2.5 cm indium–tin oxide (ITO) sheet (resistance *ca.* 20 ohm per square, from Merck) was used.

4.3.2 Molecular characterizations. FTIR spectra were taken on a Perkin Elmer 2000 FTIR spectrometer. The spectra of films were taken in reflection–absorption mode.

Matrix-assisted laser desorption ionization time-of-flight (MALDI-TOF) mass spectra were obtained by an Ultraflex II mass spectrometer (Bruker Daltonics) operating in the both positive reflection and linear modes, using 2,5-dihydroxybenzoic acid as the matrix.

Gas-phase mass determination was carried out using Agilent Technologies 7890A GC System coupled with an Agilent Technologies 5975C VL MSD with triple-axis mass detector.

Optical absorption measurements for both solutions and films were performed with a Lambda 900 Perkin-Elmer spectrometer. For solution spectra, $CHCl_3$ and chlorobenzene were used depending on the oligomer solubility, for this reason all spectra start from 300 nm. CW photoluminescence (PL) spectra were recorded using a SPEX 270 M monochromator equipped with a N_2-cooled CCD detector, by exciting with a monochromated Xe lamp. Solution PL quantum yield (QY) measurements were performed using a quinine sulfate solution (10^{-4} M sulfuric acid) as reference (QY = 54.6%) and exciting at 350 nm (QY = 54.6%). Solid-state PLQY was carried out using an integrating sphere.[42]

4.3.3 Structural and morphological analyses. XRD experiments were carried out using an Enraf Nonius CAD4 instrument for single-crystal analysis (for details see Table 6), while films and powder were examined using a computer-controlled Siemens D-500 diffractometer equipped with Soller slits and an Anton–Paar camera for variable-temperature experiments under a nitrogen atmosphere.

Morphological characterizations was performed using a commercial AFM NT-MDT apparatus in non-contact force modulation mode. Both height images and phase images were taken at the same time.

4.3.4 Calculations. All *ab initio* computations were done with Gaussian03[43] with DFT, using the three-parameter hybrid functional B3LYP.[44–46] Graphical representations of the electron orbitals were obtained with MOLEKEL.[47,48]

Molecular modelling calculations, crystal structure resolution, and packing energy minimization were performed using the Materials Studio package, release 4.0, developed by Accelrys.[39]

Table 6 Crystallographic details of **TFT**

Chemical formula	$C_{21}H_{12}OS_2$
Formula weight	344.43
Space group	$P2_1/c$ (no. 14)
a/nm	1.4862(2)
b/nm	0.5888(2)
c/nm	1.8100(3)
α (°)	90
β (°)	93.09(1)
γ (°)	90
V/nm^3	1.5815(6)
Z	4
D_{calc}/g cm^{-3}	1.447
Radiation (λ)	Mo Kα (0.71073 Å)
Temperature/K	293
Parameters refined in full-matrix least-squares	229
Unweighted agreement factor on observed data (1457)	0.056
Weighted agreement factor on observed data (1457)	0.136

4.3.5 Device preparation and measurements. OFET devices in a bottom-contact architecture were prepared by high-vacuum evaporation of the active layer, as described in ref. 14. The final pressure was 10^{-7} mbar, while the growth rate ranged from 0.1 to 0.15 Å s^{-1}, and the holder temperature was kept at 100 °C, to avoid partial re-evaporation of the compound.

The mobilities have been extracted from transfer characteristic curves in the saturation region, fitting with the standard quadratic expression: $I_{SD} = K(V_G - V_T)^2$ where $K = \frac{1}{2}\mu C_{ox}W/L$, where μ is the carrier mobility, C_{ox} (130 nm SiO_2) the capacitance per unit surface, W (15 mm) and L (3, 6, 12 μm) the width and length of the device respectively, and V_T the threshold voltage. The measurements were performed in vacuum (below 10^{-5} mbar).

The structure of bulk-heterojunction solar cells investigated in this work was indium tin oxide (ITO)/poly(3,4-ethylene-dioxythiophene)-blend-poly(styrene sulfonate) (PEDOT:PSS)/H4FT6F:PCBM (1:1 wt)/LiF/Al. On the top of pre-cleaned ITO substrates a 50 nm thick PEDOT:PSS layer was spin-coated, and subsequently substrates were baked at 100 °C for 10 min in ambient atmosphere. Then, an active layer of the solar cells was spin-coated (in glove-box) from chlorobenzene solution (20 mg mL^{-1}) on top of the PEDOT:PSS layer. Afterwards, onto the active layer, LiF and Al electrodes were thermally evaporated using vacuum deposition system at a pressure of $\sim 2 \times 10^{-6}$ mbar. The thickness of the top electrical contacts were ≈ 0.8 nm and ≈ 100 nm, respectively, while the thickness of active layer ranged from 80 to 100 nm (by AFM determination). The average area of the devices was 4.5 mm^2. Before photovoltaic characterisation, the devices were thermally annealed at 70 °C for 5 min on a calibrated hotplate in a glove-box.

Acknowledgements

The authors would like to thank Dr D. Natali and Prof. M. Sampietro of the Dipartimento di Elettronica e Informazione Politecnico Milano for OFET device measurements and helpful discussions, and S. Sitran of IENI-CNR for his technical assistance. We are also indebted to the Italian Fondazione Cariplo for partial financial support through the project "DANAE" and to the Italian MIUR through the project PRIN 2007PBWN44.

References

1 F. Jaramillo-Isaza and M. L. Turner, *J. Mater. Chem.*, 2006, **16**, 83–89.
2 F. Uckert, Y. Tak, K. Müllen and H. Bässler, *Adv. Mater.*, 2000, **12**, 905–908.
3 S. Panozzo, J.-C. Vial, Y. Kervella and O. Stephan, *J. Appl. Phys.*, 2002, **92**, 3495–3502.
4 R. Demadrille, P. Rannou, J. Bleuse, J.-L. Oddou, A. Pron and M. Zagorska, *Macromolecules*, 2003, **36**, 7045–7054.
5 X. Gong, D. Moses and A. J. Heeger, *J. Phys. Chem. B*, 2004, **108**, 8601–8605.
6 M. Sims, D. D. C. Bradley, M. Ariu, M. Koeberg, A. Asimakis, M. Grell and D. G. Lidzey, *Adv. Funct. Mater.*, 2004, **14**, 765–781..
7 K. Becker, J. M. Lupton, J. Feldmann, B. S. Nehls, F. Galbrecht, D. Q. Gao and U. Scherf, *Adv. Funct. Mater.*, 2006, **16**, 364–370.
8 X. Zhou, Y. Zhang, Y. Xie, Y. Cao and J. Pei, *Macromolecules*, 2006, **39**, 3830–3840.
9 M. Linares, L. Sciffo, R. Demadrille, P. Brocorens, D. Beljonne, R. Lazzaroni and B. Grevin, *J. Phys. Chem. C*, 2008, **112**, 6850–6859.
10 L. Sanguinet, J. C. Williams, Z. Yang, R. J. Twieg, G. Mao, K. D. Singer, G. Wiggers and R. G. Petschek, *Chem. Mater.*, 2006, **18**, 4259–4269.
11 M. Lehmann, S. W. Kang, C. Köhn, S. Haseloh, U. Kolb, D. Schollmeyer, Q. B. Wang and S. Kumar, *J. Mater. Chem.*, 2006, **16**, 4326–4334.
12 F. Lincker, N. Delbosc, S. Bailly, R. De Bettignies, M. Billon, A. Pron and R. Demadrille, *Adv. Funct. Mater.*, 2008, **18**, 3444–3453 and references cited therein.
13 W. Porzio, S. Destri, M. Pasini, U. Giovanella, T. Motta, M. D. Iosip, D. Natali, M. Sampietro, L. Franco and M. Campione, *Synth. Met.*, 2004, **146**, 259–263.
14 W. Porzio, S. Destri, U. Giovanella, M. Pasini, T. Motta, D. Natali, M. Sampietro and M. Campione, *Thin Solid Films*, 2005, **492**, 212–220.
15 M. Yoon, S. A. DiBenedetto, A. Facchetti and T. J. Marks, *J. Am. Chem. Soc.*, 2005, **127**, 1348–1349..
16 T. Lee, C. A. Landis, B. M. Dhar, B. J. Jung, J. Sun, A. Sarjeant, H. J. Lee and H. E. Katz, *J. Am. Chem. Soc.*, 2009, **131**, 1692–1705.
17 P. Scandiucci, U. Scherf, M. Collon and E. J. W. List, *E-Polymers*, 2002, **009**, 1–7.
18 T. A. M. Ferenczi, M. Sims and D. D. C. Bradley, *J. Phys. Condens. Matter.*, 2008, **20**, 045220(9).
19 Y. Liu, X. Tao, F. Wang, J. Shi, J. Sun, W. Yu, Y. Ren, D. Zou and M. Jiang, *J. Phys. Chem. C*, 2007, **111**, 6544–65.
20 J. Cornil, D. A. dos Santos, X. Crispin, R. Silbey and J. L. Brédas, *J. Am. Chem. Soc.*, 1998, **120**, 1289–1299; J. Cornil, J. P. Calbert,

 This journal is © The Royal Society of Chemistry and the Centre National de la Recherche Scientifique 2010

D. Beljonne, R. Silbey and J. L. Brédas, *Adv. Mater.*, 2000, **12**, 978–983.
21 S. R. Forrest, *Nature*, 2004, **428**, 911–918.
22 D. E. Janzen, M. W. Burand, P. C. Ewbank, T. M. Pappenfus, H. Higuchi, D. A. da Silva Filho, V. G. Young, J. L. Brédas and K. R. Mann, *J. Am. Chem. Soc.*, 2004, **126**, 15295–15308.
23 H. Meng, F. Sun, M. B. Goldfinger, G. D. Jaycox, Z. Li, W. J. Marshall and G. S. Blackman, *J. Am. Chem. Soc.*, 2005, **127**, 2406–2407.
24 J. Locklin, D. W. Li, S. C. B. Mannsfeld, E. J. Borkent, H. Meng, R. Advincula and Z. Bao, *Chem. Mater.*, 2005, **17**, 3366–3374; J. Locklin, M. E. Roberts, S. C. B. Mannsfeld and Z. Bao, *Polym. Rev.*, 2006, **46**, 79–101.
25 W. Porzio, S. Destri, M. Pasini, A. Rapallo, U. Giovanella, B. Vercelli and M. Campione, *Cryst. Growth Des.*, 2006, **6**, 1497–1503.
26 W. Porzio, M. Pasini, S. Destri, U. Giovanella and P. Fontaine, *Thin Solid Films*, 2006, **514**, 334–340.
27 E. E. Havinga, W. ten Hoeve and H. Wynberg, *Polym. Bull.*, 1992, **29**, 119–126.
28 J. Cao, J. W. Kampf and M. D. Curtis, *Chem. Mater.*, 2003, **15**, 404–411; J. Cao and M. D. Curtis, *Chem. Mater.*, 2003, **15**, 4424–4432.
29 J. Roncali, *Macromol. Rapid Commun.*, 2007, **28**, 1761–1775.
30 P. Sonar, S. P. Singh, P. Leclère, M. Surin, R. Lazzaroni, T. T. Lin, A. Dodabalapur and A. Sellinger, *J. Mater. Chem.*, 2009, **19**, 3228–3237.
31 C. Wang, M. E. Benz, E. Le Goff, J. L. Schlinder, J. Allbritton-Thomas, C. N. Kannewurf and M. G. Kanatzidis, *Chem. Mater.*, 1994, **6**, 401–410.
32 G. Zotti, S. Zecchin, B. Vercelli, M. Pasini, S. Destri, F. Bertini and A. Berlin, *Chem. Mater.*, 2006, **18**, 3151–3161.
33 A. F. Diaz, J. Crowley, J. Bargon, G. P. Gardini and J. B. Tottance, *J. Electroanal. Chem.*, 1981, **121**, 355–61.
34 S. Zecchin, G. Schiavon, R. Tomat and G. Zotti, *J. Electroanal. Chem.*, 1986, **215**, 377–383.
35 G. Zotti, S. Zecchin, G. Schiavon and B. Vercelli, *J. Electroanal. Chem.*, 2005, **575**, 169–175.
36 W. Porzio, S. Destri, M. Pasini, U. Giovanella, R. Resel, O. Werzer, G. Scavia, L. Fumagalli, D. Natali and M. Sampietro, *Synth. Met.*, 2009, **159**, 513–517.
37 M. D. Levi, R. Demadrille, E. Markevich, Y. Gofer, A. Pron and D. Aurbach, *Electrochem. Commun.*, 2006, **8**, 993–998.
38 I. F. Perepichka, S. Roquet, P. Leriche, J. M. Raimundo, P. Frère and J. Roncali, *Chem.–Eur. J.*, 2006, **12**, 2960–2966.
39 *MATSTUDIO Modeling*, release 4.0, Accelrys Inc., USA, 2003 (www.accelrys.com).
40 C. Winder, D. Muhlbacher, H. Neugebauer, N. S. Sariciftci, C. Brabec, R. A. J. Janssen and J. K. Hummelen, *Mol. Cryst. Liq. Cryst.*, 2002, **385**, 213–220.
41 H. Pan, Y. Li, Y. Wu, P. Liu, Beng S. Ong, Shiping Zhu and Gu Xu, *J. Am. Chem. Soc.*, 2007, **129**, 4112–4113.
42 J. Moreau, U. Giovanella, J.-P. Bombenger, W. Porzio, V. Vohra, L. Spadacini, G. Di Silvestro, L. Barba, G. Arrighetti, S. Destri, M. Pasini, M. Saba, F. Quochi, A. Mura, G. Bongiovanni, M. Fiorini, M. Uslenghi and C. Botta, *ChemPhysChem*, 2009, **10**, 647–653.
43 M. J. Frisch, G. W. Trucks, H. B. Schlegel, G. E. Scuseria, M. A. Robb, J. R. Cheeseman, J. A. Montgomery, Jr., T. Vreven, K. N. Kudin, J. C. Burant, J. M. Millam, S. S. Iyengar, J. Tomasi, V. Barone, B. Mennucci, M. Cossi, G. Scalmani, N. Rega, G. A. Petersson, H. Nakatsuji, M. Hada, M. Ehara, K. Toyota, R. Fukuda, J. Hasegawa, M. Ishida, T. Nakajima, Y. Honda, O. Kitao, H. Nakai, M. Klene, X. Li, J. E. Knox, H. P. Hratchian, J. B. Cross, C. Adamo, J. Jaramillo, R. Gomperts, R. E. Stratmann, O. Yazyev, A. J. Austin, R. Cammi, C. Pomelli, J. W. Ochterski, P. Y. Ayala, K. Morokuma, G. A. Voth, P. Salvador, J. J. Dannenberg, V. G. Zakrzewski, S. Dapprich, A. D. Daniels, M. C. Strain, O. Farkas, D. K. Malick, A. D. Rabuck, K. Raghavachari, J. B. Foresman, J. V. Ortiz, Q. Cui, A. G. Baboul, S. Clifford, J. Cioslowski, B. B. Stefanov, G. Liu, A. Liashenko, P. Piskorz, I. Komaromi, R. L. Martin, D. J. Fox, T. Keith, M. A. Al-Laham, C. Y. Peng, A. Nanayakkara, M. Challacombe, P. M. W. Gill, B. Johnson, W. Chen, M. W. Wong, C. Gonzalez and J. A. Pople, *GAUSSIAN 03, Revision C.02*, Gaussian, Inc., Wallingford CT, 2004.
44 A. D. Becke, *Phys. Rev. A: At., Mol., Opt. Phys.*, 1988, **38**, 3098–3100.
45 A. D. Becke, *J. Chem. Phys.*, 1993, **98**, 5648–5652.
46 C. Lee, W. Yang and R. G. Parr, *Phys. Rev. B*, 1988, **37**, 785–789.
47 P. Flükiger, H. P. Lüthi, S. Portmann and J. Weber, *MOLEKEL 4.3*, Swiss Centre for Scientific Computing, Manno, Switzerland, 2000–2002.
48 S. Portmann and H. P. Lüthi, MOLEKEL: An Interactive Molecular Graphics Tool, *Chimia*, 2000, **54**, 766–771.